Received: 21 August 2026; **Revised:** 21 October 2026; **Accepted:** 13 November 2026; **Published:** 20 November 2026
Archs Sci. (2026) Volume 76, Issue 5 Pages 263-272, Paper ID 2026527.
https://doi.org/10.68304/as/76527

Degradation Mechanisms of Concrete Following High-Temperature Exposure and Different Cooling Methods

Shaojun Fu[1] and Hao Yuan[1,*]
[1]Shaanxi Key Laboratory of Safety and Durability of Concrete Structures, Xijing University, Xi'an, Shaanxi 710123, China
Correspondence: 15095803430@163.com

Abstract
High-temperature exposure substantially alters the physical and mechanical properties of concrete, and understanding the underlying degradation mechanisms can provide an important basis for post-fire assessment, emergency response, and repair decisions. In this study, concrete specimens were heated to ten target temperatures (200, 300, 350, 400, 450, 500, 550, 600, 700, and 800°C) and subsequently subjected to either natural cooling or water cooling. After the specimens had cooled and dried, their surface color, mass, relative dynamic modulus of elasticity, electrical resistance, and compressive strength were measured. Surface alkalinity was assessed by observing color changes following the application of phenolphthalein, while the CIE-$L^*a^*b^*$ color system provided a quantitative description of changes in surface appearance. The findings indicate an association between phenolphthalein-induced surface color and the presence of $Ca(OH)_2$; more intense coloration is consistent with a stronger alkaline response, although the color alone does not directly quantify the compound's concentration. Mass loss increased with heating temperature, principally reflecting moisture loss and subsequent thermally induced decomposition of hydration products. The development of cracking and changes in moisture state also influenced electrical resistance. With increasing temperature, resistance rose after natural cooling but declined after water cooling, indicating that the cooling procedure influenced the electrical response. Both relative dynamic modulus of elasticity and residual compressive strength decreased as exposure temperature increased, with particularly severe deterioration in the 600–800°C range. Taken together, the measured variables provide complementary indicators of post-heating damage and show why the cooling history must be considered when assessing the condition of fire-exposed concrete.

Index Terms Concrete; Elevated temperature; Cooling methods; Compressive strength; Electrical resistance; Ultrasonic testing

I. Introduction
Concrete is among the most widely used structural materials, and its behavior under elevated temperatures remains an important research topic because of the consequences of fires for structural safety. Over recent decades, numerous studies have examined the thermal, physical, and mechanical behavior of concrete exposed to high temperatures [1]–[7]. Elevated temperature changes the moisture content, chemical composition, pore structure, and integrity of the cementitious matrix; these changes may progressively compromise mechanical performance and durability. Geng et al. [2] investigated high-temperature damage in calcareous-aggregate concrete, including its mechanical response and acoustic-emission behavior. Kizilkanat et al. [8] demonstrated that thermal conductivity depends on the material composition and reported no marked change in their investigated concretes below approximately 300°C. Such findings illustrate that concrete is a heterogeneous, multiphase composite whose response cannot be described by exposure temperature alone. Aggregate mineralogy, cement hydration products, moisture availability, heating duration, and the cooling procedure all contribute to the magnitude and evolution of damage. Accordingly, evaluations of post-fire strength should examine both the thermal exposure and the conditions under which the heated material returns to ambient temperature.

After high-temperature exposure, concrete can be cooled naturally in air or rapidly by applying water, and the selected cooling method may substantially change its subsequent behavior. Previous research has addressed the consequences of heating and cooling under different combinations of material properties and environmental conditions. Eurocode 2 [9] provides design provisions concerning the behavior of concrete structures in fire, including temperature-dependent material characteristics that are relevant to structural assessment. Yan et al. [10], Jia et al. [11], and Lü et al. [12] investigated aspects of mechanical or microstructural degradation following elevated-temperature exposure and associated cooling conditions. Their findings emphasize that residual performance depends on both the severity of heating and the environment during cooling. Bi et al. [13] examined the effects of

ARCHIVES DES SCIENCES
A Multidisciplinary Journal

natural and water cooling on the dynamic behavior of ordinary concrete, while Karolina and Corsika [14] discussed the mechanical and physical behavior of fire-exposed concrete. Cioni et al. [15] investigated the assessment of fire damage to reinforced-concrete elements, highlighting the importance of identifying the consequences of a thermal event for subsequent structural evaluation. Du et al. [16] studied temperature-related color changes and residual strength in tunnel-lining concrete, providing a basis for comparing visual indicators with mechanical deterioration. Sun et al. [17], Hu et al. [18], and Zhang et al. [19] likewise examined thermal changes in concrete or related cement-based materials, including variations in wave velocity, surface color, and thermal performance. These investigations are relevant because damage associated with dehydration, mineral transformations, and cracking often becomes more pronounced as temperature increases through the intermediate and upper parts of the investigated range. Chan et al. [20] found that rapid cooling could cause additional strength deterioration through thermal shock, compared with more gradual cooling, in their tested concretes. Bingöl and Gül [21] also evaluated residual properties under different cooling regimes. Nevertheless, the effect is not uniform across every concrete mixture: Karakoç [22] reported that, for the particular lightweight-aggregate mixtures in that investigation, the average strength reductions under water, furnace, and natural cooling were 78%, 81%, and 83%, respectively. These results should therefore be interpreted in relation to the composition and conditions of each experiment, rather than treated as a universal ranking of cooling procedures.

Although many investigations have addressed fire-induced damage and residual strength, fewer studies have jointly examined the effects of heating temperature and cooling procedure using several complementary measurements on the same concrete mixture [21]–[27]. Further experimental evidence is valuable because visual deterioration, loss of mass, electrical response, ultrasonic propagation, and compressive strength are governed by related but not identical aspects of material degradation. In practice, an evaluation based on only one indicator may not capture the influence of moisture redistribution, microcracking, or the chemical decomposition of the cement matrix. The present investigation therefore compares concrete specimens subjected to prescribed heating regimes and then cooled naturally or by immersion in water. Its objective is to characterize changes in mass, surface color, electrical resistance, relative dynamic modulus of elasticity, and compressive strength, and to examine relationships among these indicators. This approach approximates certain aspects of concrete that has experienced heating followed by water-based firefighting or natural cooling, although a furnace experiment does not reproduce all the thermal gradients and mechanical restraints present in a real structure. The results are intended to inform post-fire damage assessment and interpretation of residual material performance under clearly specified experimental conditions.

II. Materials and Methods

A. Materials and Mix Proportions of Concrete

The cement used in this investigation was Conch-brand P · O 42.5 ordinary Portland cement. Its reported chemical composition and basic physical properties are presented in Tables 1 and 2, respectively.

Table 1: Chemical Composition of Cement (%)

Cement type	CaO	SiO2	Al2O3	Fe2O3	TiO2	MgO	SO3	Na2O	Loss on ignition
P·O 42.5	8.93	48.50	25.36	5.12	0.57	1.15	1.15	0.52	0.79

Table 2: Basic Properties of Cement

Standard consistency (%)	25.3
Initial setting time (min)	$\geq$45
Final setting time (min)	$\leq$600
Soundness	Qualified
Compressive strength (MPa)	58.3
Density (g/cm^3)	3.11

Grade I fly ash supplied by Henan Sitong Chemical Construction Co., Ltd., was incorporated into the mixture, and its reported technical indices are summarized in Table 3. Natural river sand with a fineness modulus of 2.58 served as the fine aggregate and was classified as medium sand. The coarse aggregate consisted of continuously graded crushed stone with particle sizes ranging from 5 to 30 mm. A superplasticizer and an air-entraining agent manufactured by Jiangsu Sobute New Materials Co., Ltd., were included to provide the specified workability and air-entrainment characteristics. Ordinary tap water was used for mixing. These constituent details are important when interpreting the high-temperature results, because the binder composition, aggregate grading, and initial moisture conditions can all affect subsequent dehydration, thermal expansion, cracking, and residual mechanical strength.

Table 3: Technical Indices of Fly Ash

Fineness	10.2%
Water requirement ratio	92%
Loss on ignition	4.3%
Water content	0.56%
SO3	1.18%

Table 4: Concrete Mix Proportions (kg/m^3)

Cement type	P·O 42.5
Cement	202
Fly ash	87
Sand	688
Water	130
Coarse aggregate (small)	389
Coarse aggregate (medium)	505
Coarse aggregate (large)	355
Water-reducing agent	1.19
Air-entraining agent	0.02

Concrete specimens were cast as cubes measuring 100 mm $\times$ 100 mm $\times$ 100 mm. The proportions of the cement, fly ash, aggregates, water, and admixtures used to prepare the specimens are reported in Table 4, with material quantities

ARCHIVES DES SCIENCES
A Multidisciplinary Journal

expressed per cubic meter of concrete. The mixture was held constant across the temperature and cooling comparisons so that the interpretation could focus on the thermal treatment and cooling procedure.

B. Specimen Design and Test Methods

Considering different temperatures (200, 300, 350, 400, 450, 500, 550, 600, 700, 800°C) and cooling methods (natural cooling and water cooling), 10 groups of cube compressive specimens were designed, with 4 in each group and a total of 80 specimens, which were used to measure the compressive strength,mass loss,relative dynamic modulus of elasticity,resistance and chromaticity of concrete cube after high temperature. LYL-17TL, a high temperature trolley furnace manufactured by Luoyang Liyu cellar furnace Co., Ltd., is used for this high temperature test (Figure 1).



Figure 1: High-Temperature Trolley Furnace

The rated voltage is 380V, the power is 70kw, the maximum target temperature can reach 1200°C, the temperature control accuracy is ±1°C, the internal net space size is 1200mm*800mm*800mm, and the temperature is controlled by the supporting temperature control cabinet.According to the actual situation of the test and safety factors,the linear heating mode is adopted,and the heating rate is set at 5°C/min. The test pieces of different groups are heated to the target temperature respectively. Due to the small size of the test piece, the internal and external temperatures of the test pieces are kept the same after reaching the target temperature for 1 hour. At the same time, taking 400°C as the benchmark, after the temperature before 400°C is constant, the power supply of the high temperature trolley furnace is cut off, the furnace door is opened, and the heated test pieces are taken out. After 400°C, the samples are taken out when the furnace temperature after 400°C is reduced to 400°C. The specimens cooled naturally are put into the empty stainless steel basin, and the specimens cooled by soaking in water are put into the basin connected with tap water in advance, and the specimens are cooled to room temperature.

Specimen mass and electrical resistance were measured before and after heating. Mass was recorded using a TCS-60 electronic platform balance with a stated precision of 0.01 g. A Tonghui TH2811D digital bridge LCR instrument was used to measure the electrical response of the concrete specimens; the instrument and the measurement process are illustrated in Figure 2.

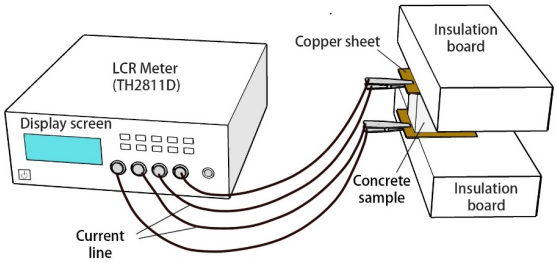


Figure 2: LCR Meter and Electrical Measurement Procedure

The relative dynamic modulus of elasticity was estimated from ultrasonic measurements performed with an N-M-4A nonmetallic ultrasonic testing analyzer. Following heating and cooling, phenolphthalein reagent was applied to the specimen surfaces, and temperature-dependent changes in the resulting coloration were recorded. Compressive strength was measured with a 2,000-kN microcomputer-controlled electrohydraulic servo testing machine, illustrated in Figure 3. The reported loading rate was 0.5 kN/s under the stated test setting. These tests provided complementary measurements of material condition: mass loss reflected changes associated with moisture and decomposition, ultrasonic response provided an index of internal deterioration, electrical measurement was sensitive to moisture and connected pore structure, and compression testing quantified the remaining load-bearing capacity of the concrete cubes.

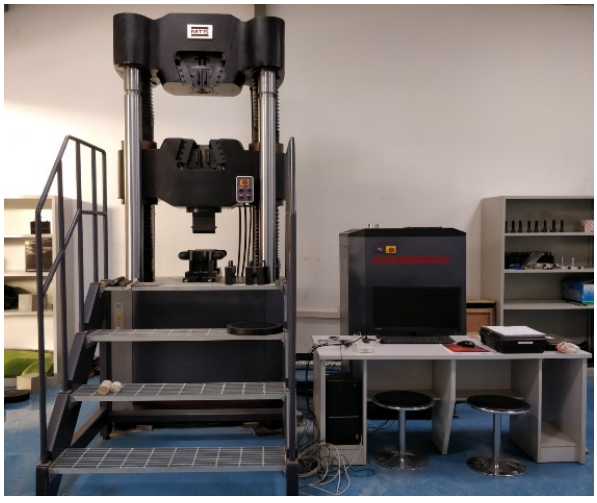


Figure 3: Compressive-Strength Testing Machine

ARCHIVES DES SCIENCES
A Multidisciplinary Journal

III. Results

A. Surface Color Characteristics

Concrete contains calcium hydroxide, $Ca(OH)_2$, together with other hydration products and, where carbonation has occurred, calcium carbonate, $CaCO_3$. Phenolphthalein provides a qualitative indication of the alkalinity of the surface region: sufficiently alkaline material develops a pink-to-red coloration after contact with the indicator, while less alkaline regions may remain substantially colorless. Following exposure to the various heating temperatures and subsequent cooling, the indicator was applied to the concrete surfaces, and the visible response was assessed after approximately 10 min. Surface appearance was also characterized using a TES-135A colorimeter in the CIE-$L^*a^*b^*$ color space. Within this system, L^* describes lightness on a scale from black to white, a^* describes the green-to-red axis, and b^* describes the blue-to-yellow axis. Using instrumental color coordinates alongside visual observations facilitates a more consistent comparison of specimens; however, changes in phenolphthalein color must not be interpreted as direct quantitative measurements of the amount of calcium hydroxide without independent chemical analysis.

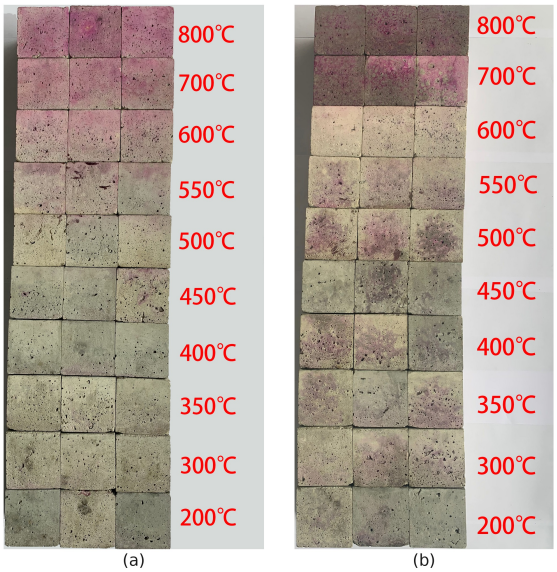


Figure 4: Surface Color Following Phenolphthalein Treatment: (a) Natural Cooling; (b) Water Cooling

After the heated specimens had cooled, the phenolphthalein solution was applied uniformly to the exposed surfaces. Figure 4 compares the coloration obtained for the natural-cooling and water-cooling conditions. For the naturally cooled specimens, the red response generally became more apparent as exposure temperature increased, particularly from approximately 500°C onward. The specimens subjected to water cooling also exhibited a pronounced change in coloration over the temperature range. The two cooling histories therefore produced visibly different surface responses, which may reflect differences in alkalinity, water penetration, and the subsequent transformation of hydration products. As an observational result, the color trend is useful for identifying changes in post-heating condition, but it should be interpreted together with the instrumental color measurements and mechanical testing rather than used as a stand-alone measure of structural safety.

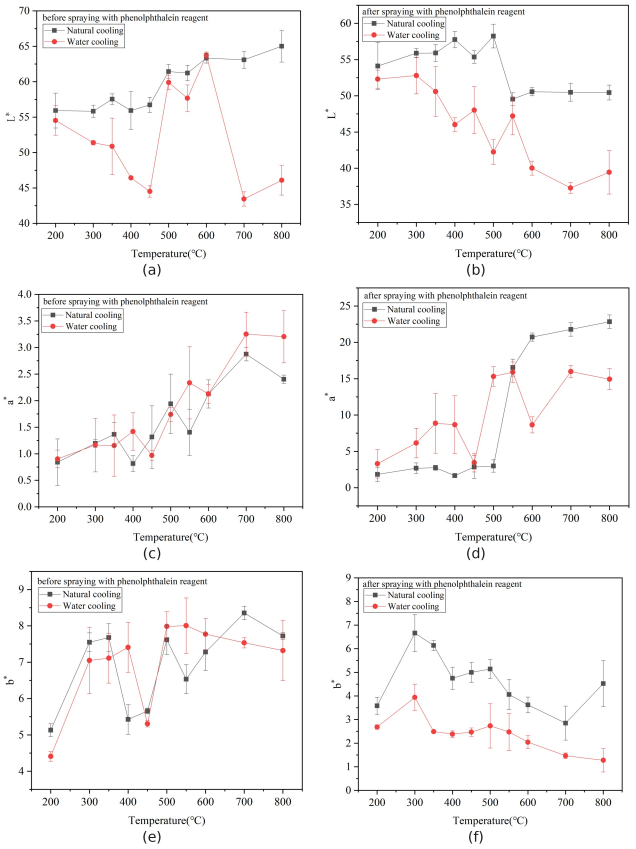


Figure 5: CIE-L*a*b* Color Coordinates Before and After Phenolphthalein Treatment: (a, b) Lightness; (c, d) Red–Green; (e, f) Yellow–Blue

Figure 5 presents the changes in the CIE-$L^*a^*b^*$ coordinates of the concrete surfaces before and after phenolphthalein treatment. In panels (a) and (b), the L^* values associated with natural cooling were generally higher than those associated with water cooling, with the minimum observed values occurring at approximately 700°C. Panels (c) and (d) show the temperature-related evolution of the a^* coordinate. Before the indicator was applied, a^* generally increased and reached a maximum near 700°C; after treatment, the value increased substantially around 450°C and attained its highest reported value at 800°C. Panels (e) and (f) describe the b^* coordinate: before phenolphthalein application, the peak occurred near 700°C, whereas after application, the maximum occurred at approximately 300°C and the parameter declined gradually from around 500°C. The different temperature trajectories of the three coordinates indicate that lightness, redness, and yellowness did not respond identically to heating or chemical

ARCHIVES DES SCIENCES
A Multidisciplinary Journal

treatment. Accordingly, the full color response provides more informative evidence than a single visual description of the surface becoming darker or redder.

B. Changes in Mass and Relative Dynamic Modulus of Elasticity

As the heating temperature increased, dehydration, decomposition, and the growth of cracks altered the specimen mass and internal structure. To express these changes consistently, the mass-loss ratio of each specimen was calculated relative to its mass before heating, as specified in Equation (1). This ratio supplies a common basis for comparing specimens exposed to different heating temperatures and cooling procedures.

$$\xi = \frac{m_0 - m_1}{m_0} \times 100\%, \tag{1}$$

Here, ξ denotes mass loss as a percentage, m_0 is the specimen mass before heating, and m_1 is the mass measured after heating and cooling. Figure 6 presents the resulting dependence on exposure temperature. The precise timing of the mass measurement relative to wet cooling should be documented, because residual water can influence the observed ratio.

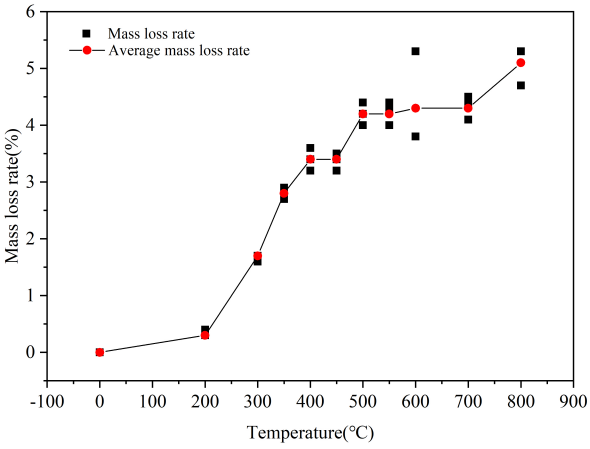


Figure 6: Mass-Loss Ratio Following Exposure to Different Temperatures

The mass-loss results in Figure 6 show a clear dependence on the maximum heating temperature. Loss became appreciable after exposure to approximately 200°C and increased markedly over the interval extending from room temperature to 500°C. From approximately 500 to 700°C, the corresponding curve was relatively flat, suggesting that the rate of additional loss was smaller over this intermediate interval in the reported measurements. Between 700 and 800°C, mass loss increased further and more rapidly than over the preceding 500–700°C interval. This nonuniform trajectory is consistent with different temperature ranges activating different physical and chemical processes, including the evaporation of moisture and the decomposition of constituents within the hardened cement paste. Although evaporation of free water contributes to the early changes, the higher-temperature loss should not be attributed solely to free water because chemically bound water and other decomposition products may also contribute.

Ultrasonic pulse velocity provides a widely used, nondestructive means of evaluating the internal condition and apparent continuity of concrete. The relative dynamic modulus of elasticity was used here to characterize the extent of internal damage and changes in the apparent stiffness following high-temperature exposure, with interpretation dependent on specimen moisture and measurement conditions. The relative dynamic modulus was calculated from the ratio of the measured ultrasonic velocities, as shown in Equation (2).

$$E = \left(\frac{V_t}{V_0}\right)^2 = \left(\frac{T_0}{T_t}\right)^2, \tag{2}$$

where E denotes the relative dynamic modulus, V_0 and V_t are the ultrasonic longitudinal-wave velocities (km/s) before and after heating, and T_0 and T_t are the corresponding pulse transit times for a fixed propagation path. The subscript t identifies the selected heating temperature. The squared relationship is interpreted as a relative measure under the assumption that density changes have not been explicitly incorporated into the calculation.

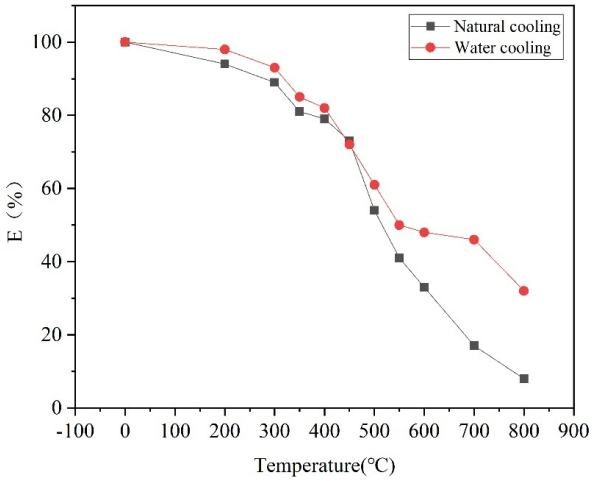


Figure 7: Relative Dynamic Modulus of Elasticity After Heating

The relative dynamic modulus of elasticity varied with both the maximum heating temperature and the cooling method, as illustrated in Figure 7. Under both cooling conditions, the modulus declined comparatively slowly before approximately 450°C, followed by a more rapid decline as temperature increased. At 450°C, the relative modulus after either cooling procedure was approximately 72% of the reference value. At 550°C, the corresponding reported values were 54% after natural cooling and 61% after water cooling. By 800°C, they had declined to approximately 8% and 32%, respectively. These substantial reductions indicate pronounced changes in ultrasonic wave propagation and are consistent with extensive loss of internal continuity due to cracking, damage to the cement matrix, and thermally induced microstructural changes. The consistently lower relative modulus observed

ARCHIVES DES SCIENCES
A Multidisciplinary Journal

for the naturally cooled specimens at the upper temperatures is an experimental feature that should be assessed separately from the residual compressive-strength ranking, because the two response variables are influenced differently by moisture and damage.

C. Changes in Electrical Resistance Following Different Cooling Methods

Figure 8 compares the measured electrical resistance after natural cooling and water cooling at four excitation frequencies: 100, 120, 1,000, and 10,000 Hz. In the naturally cooled specimens, resistance increased as the maximum heating temperature rose, whereas the water-cooled specimens showed the opposite tendency. At 200°C, naturally cooled specimens exhibited resistances of 22.54, 20.49, 4.35, and 0.31 MΩ at the four respective frequencies. At 500°C, the corresponding values increased to 76.57, 68.4, 44.19, and 15.93 MΩ; at 800°C, they reached 97.11, 85.62, 47.43, and 17.56 MΩ. These measurements indicate a substantial increase in resistance after natural cooling, particularly at the lower frequencies. Conversely, water-cooled specimens exhibited values of 10.7, 9.9, 3.24, and 0.18 MΩ at 200°C, falling to 0.07, 0.07, 0.05, and 0.03 MΩ at 500°C. By 800°C, the reported resistances were only 0.0018, 0.0018, 0.0013, and 0.0011 MΩ, respectively. These contrasting results suggest that thermal cracking, the extent of drying, and subsequent penetration or retention of water jointly influenced the electrical response. Resistance also decreased as the measurement frequency increased, indicating that frequency must be reported alongside any electrical test result. Consequently, electrical resistance may help distinguish different post-heating states, but the effect of moisture makes comparisons between cooling procedures dependent on specimen conditioning.

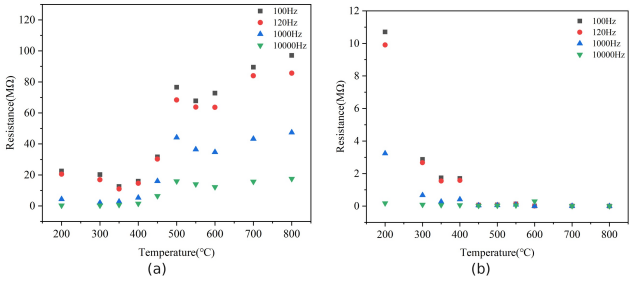


Figure 8: Electrical Resistance After Heating and Cooling: (a) Natural Cooling; (b) Water Cooling

D. Compressive Strength

Figure 9 illustrates the residual cube compressive strength of concrete following heating and the two cooling procedures. At every reported target temperature, the naturally cooled specimens retained higher compressive strength than the water-cooled specimens. At 200°C, residual strength was 55.83 MPa after natural cooling and 40.4 MPa after water cooling. The strength of both sets subsequently declined as maximum exposure temperature increased, although the rate of reduction was not uniform. Based on the slopes of the reported strength curves, three intervals can be distinguished. In the first interval, from 200 to 400°C, natural-cooling strength decreased from 55.83 to 44.07 MPa, corresponding to a reduction of 21.06%; the water-cooling value fell from 40.4 to 33.83 MPa, a reduction of 16.26%. These decreases show that measurable deterioration had already occurred even where surface cracking was not yet conspicuous. In the second interval, from 400 to 600°C, naturally cooled specimens declined from 44.07 to 34.9 MPa, or 20.8%, while water-cooled specimens declined from 33.83 to 28.43 MPa, or 15.96%. At 400°C, the specimen surfaces showed no prominent cracks; by 600°C, visible cracks had developed, suggesting substantially greater internal structural deterioration. In the third interval, from 600 to 800°C, the strengths decreased from 34.9 to 22.57 MPa after natural cooling and from 28.43 to 17.71 MPa after water cooling. The corresponding reductions were 35.33% and 37.71%, respectively. Cracks at 800°C were visibly wider and more extensive than those at 600°C, providing a qualitative explanation for the steeper loss of load-bearing capacity in the final interval. Overall, the comparative trend emphasizes the importance of identifying the cooling history when using residual strength to assess the condition of concrete following fire exposure.

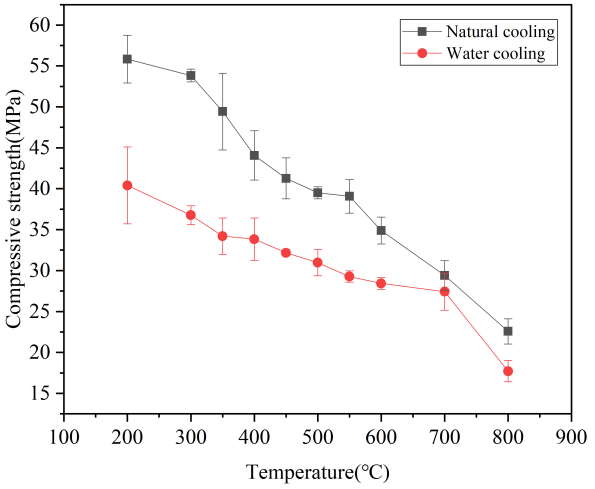


Figure 9: Residual Cube Compressive Strength at Different Temperatures

IV. Discussion

Heating alters the principal constituents and microstructure of the cementitious matrix, including calcium hydroxide, $Ca(OH)_2$, calcium carbonate, $CaCO_3$, and calcium silicate hydrate (C–S–H) [28]. Different changes dominate at different temperatures. Near 100–120°C, evaporable water is progressively released from the pore structure. At higher temperatures, some chemically bound water is lost as hydration products become unstable; additional dehydration and decomposition of C–S–H and related phases can occur over the approx-

imate 180–300°C range and beyond [29]. Calcium hydroxide decomposes over a broad interval centered approximately on 450–550°C, producing calcium oxide, CaO, and water. At still higher temperatures, calcium carbonate can decompose into CaO and carbon dioxide, although the precise onset and extent of these reactions depend on the material composition, thermal history, and local conditions. These overlapping transformations should therefore be regarded as temperature-dependent mechanisms rather than reactions occurring instantaneously at one universal temperature. Their cumulative effect includes changes in porosity, internal cracking, and the ability of concrete to withstand mechanical loading after cooling.

As temperature increases, the quantity and distribution of calcium hydroxide may change through dehydration and subsequent rehydration. Calcium oxide formed during heating can react with moisture from the atmosphere or cooling water to form calcium hydroxide again, while carbonate decomposition may contribute additional calcium oxide at sufficiently high temperatures [30]. The pronounced phenolphthalein coloration observed after some high-temperature treatments may thus reflect the combined effects of residual alkalinity, thermally induced chemical changes, and exposure to water during cooling. Changes in the CIE-L*a*b* coordinates were less uniform than the overall visual impression, with appreciable differences emerging over the higher-temperature part of the test range, particularly around and above 550°C. Because phenolphthalein is an indicator of pH rather than a direct measure of calcium hydroxide concentration, a darkened or intensified color cannot independently identify the amount of a specific hydration product. Nevertheless, the changes in surface appearance provide useful supporting information when considered alongside mass loss, ultrasonic response, and compressive strength.

The quality change of concrete is mainly related to evaporation of internal free water. With the increase of temperature, the mass loss rate is rising. The mass loss rate is the biggest change between 200°C and 500°C, and the mass loss is usually caused by evaporation of free water in the sample. The mass loss rate slows down between 500°C and 700°C, which is mainly due to the slow loss of crystal water,when the temperature is over 700°C,$CaCO_3 \rightarrow CaO + CO_2$, which leads to quality loss. Generally speaking, when the temperature reaches a certain level, the surface of concrete will peel off. However, in this study, no obvious peeling phenomenon was found after different high temperature. Luo et al., [30]found that when the temperature reached 800°C or 1100°C, there was no obvious spalling phenomenon of concrete after heating and cooling. This phenomenon is considered to be related to the secondary hydration of different components in concrete, such as $Ca(OH)_2$ produced by the secondary reaction mentioned above. When heated, the moisture of concrete sample is sufficient, so the secondary hydration of concrete is complete. The relationship between mass loss rate, relative dynamic modulus of elasticity and compressive strength is shown in Figure 10–12. In Figure 10 and 11, the change direction of mass loss rate and compressive strength after heat treatment at different temperatures is the same, showing a linear relationship. In Figure 11, the mass loss rate and the relative dynamic modulus of elasticity change in parallel as the temperature increases. Therefore, the mass loss rate can be used to evaluate the relative dynamic modulus of elasticity and compressive strength, as shown in Eqs. (3)–(6).

$$\sigma = 63.2 - 6.59\xi \qquad R^2 = 0.82, \tag{3}$$

$$\sigma = 40.9 - 4.64\xi \qquad R^2 = 0.87, \tag{4}$$

$$\xi = 1.21 - 0.16v \qquad R^2 = 0.70, \tag{5}$$

$$\xi = 1.09 - 0.98v \qquad R^2 = 0.97. \tag{6}$$

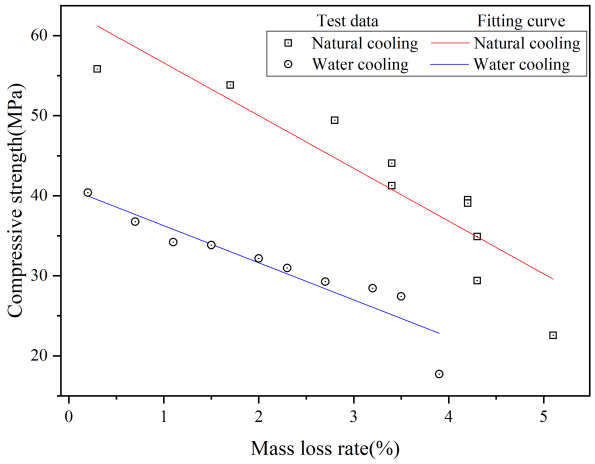


Figure 10: Relationship Between Mass Loss and Compressive Strength

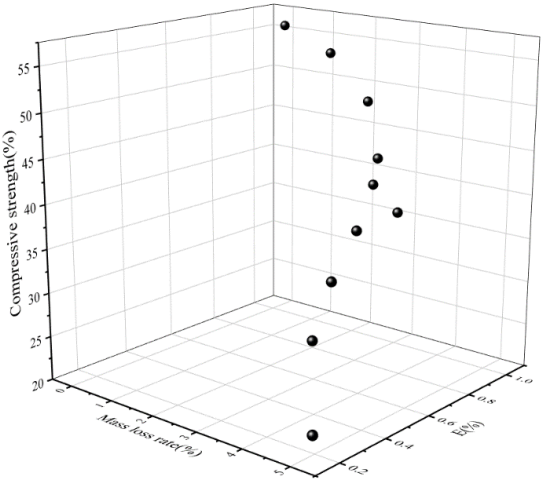


Figure 11: Three-Dimensional Relationship Among Mass Loss, Relative Dynamic Modulus, and Compressive Strength

Exposure to elevated temperatures can substantially reduce both the mechanical performance and durability of concrete, particularly through changes in the cement matrix and the development of internal cracking. The relative dynamic modulus

ARCHIVES DES SCIENCES
A Multidisciplinary Journal

of elasticity provides a nondestructive indicator of damage, although its dependence on moisture and propagation conditions warrants attention. A larger measured relative modulus generally indicates a more continuous internal structure, whereas a lower value is compatible with accumulated damage. Before 450°C, the elastic modulus of natural cooling and water cooling decreased slowly. After 450°C, the elastic modulus decreased rapidly after two cooling methods, and the modulus of elasticity under natural cooling was always smaller than that under water cooling. Before the high temperature of 450°C, due to the evaporation of free water in the concrete, the pores will be exposed, and the porosity will increase. However, combined with the existing references, it is shown that the residual unhydrated cement particles will have secondary hydration at this time, thus filling part of the pores. After the high temperature of 450°C, the hydration products of the concrete will continue to dehydrate and decompose. The expansion and deformation of concrete during fire and high temperature are mainly divided into 4 aspects: thermal expansion of coarse aggregate, shrinkage of hydration products, internal damage of coarse aggregate, cracks at the interface between C-S-H gel and aggregate.

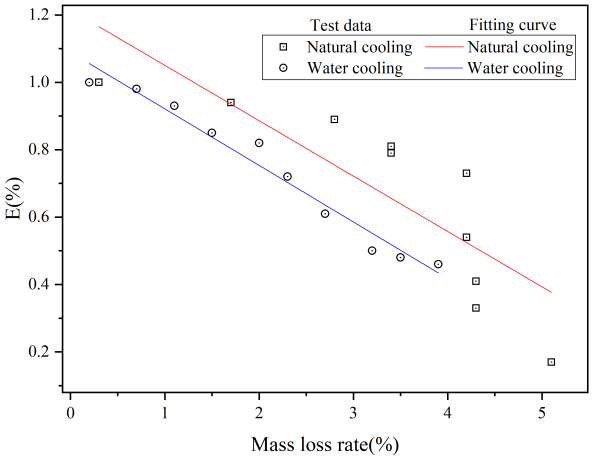


Figure 12: Relationship Between Mass Loss and Relative Dynamic Modulus

After natural cooling, the expansion of coarse aggregate can be recovered, but the other three kinds of deformation can not be recovered. After the fire, high temperature leads to the increase of internal porosity of concrete, which reduces the compactness of concrete, so the relative dynamic elastic modulus of concrete decreases significantly. With the increase of temperature, the relative dynamic elastic modulus and compressive strength of concrete show a downward trend, and the change direction of relative dynamic elastic modulus and compressive strength is the same after heating at different temperatures. Therefore, the relative dynamic modulus of elasticity can be used to evaluate the compressive strength value (Figure 13), as shown in Eqs. (7) and (8).

$$\sigma = 17.40 + 35.67v \qquad R^2 = 0.93, \tag{7}$$

$$\sigma = 12.14 + 25.82v \qquad R^2 = 0.78. \tag{8}$$

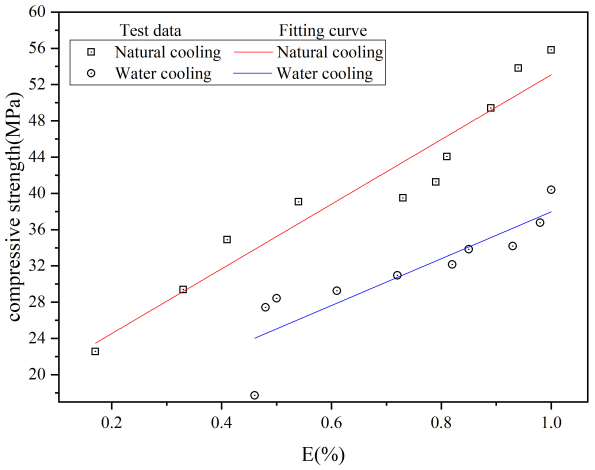


Figure 13: Relationship Between Relative Dynamic Modulus and Compressive Strength

The experiments showed that thermal exposure changed the physical and electrical properties of the concrete specimens in ways that depended on both the heating temperature and subsequent cooling. At about 200°C, the surface characteristics of concrete samples basically remain unchanged, and the resistance at this stage is closely related to temperature. Evaporation of pore water and changes in pore connectivity may increase resistance in naturally cooled material; the response after water cooling is different because moisture can penetrate cracks and interconnected pores. With the increase of temperature, in the temperature range of 200°C-600°C, the moisture in the concrete sample gradually disappears. In the temperature range of 600°C-800°C, some carbonate minerals in concrete begin to decompose after 600 °C, especially $CaCO_3$. The hot crack will expand with the increase of temperature. After 600°C, the hot crack will be more obvious. The increase of crack under natural cooling will lead to the increase of resistance. The increase of temperature and crack under water cooling will lead to the penetration of cooling water into the concrete, so the resistance will continue to decrease. At the same time, four different frequencies (100, 120, 1000, 10000Hz) were used to measure the concrete samples heated at different temperatures. With the increase of frequency, the resistance of concrete samples heated at the same temperature decreases. When the frequency reaches 10000Hz, the resistance of the samples heated at different temperatures has a small change. Previous work on AC impedance measurement in cement-based materials by Wang et al. [31] and Shen et al. [32] establishes that the measured electrical response is sensitive to frequency, moisture distribution, and microstructural changes, providing relevant context for the trends observed here.

The reduction in compressive strength with increasing exposure temperature is associated with the gradual degradation of the concrete's internal structure. Heating causes the loss of

free and chemically bound water, alters the hydration products, and may increase pore volume and microcrack density. Thermal incompatibility between aggregates and cement paste can further promote cracking at their interfaces, particularly during heating and cooling transitions. Together, these effects reduce the ability of the material to transfer and sustain compressive stress. The strength measurements reported in this study demonstrate a pronounced loss of residual capacity at the highest temperatures and show that the damage associated with water cooling can differ from that after natural cooling. Accordingly, the interpretation of compressive strength should be supported by evidence from the associated physical measurements rather than based solely on the maximum temperature.

V. Conclusion

The present study investigated the physical and mechanical deterioration of concrete specimens heated to different temperatures and subsequently subjected to natural cooling or water cooling. Surface appearance before and after phenolphthalein treatment, mass loss, electrical resistance, relative dynamic modulus of elasticity, and residual compressive strength were evaluated together. The combined measurements reveal several complementary aspects of the degradation process and show the importance of cooling procedure in post-heating assessment. The principal findings are summarized below, with the observations restricted to the mixture and exposure conditions investigated.

(1) Following natural cooling or water cooling, the phenolphthalein-treated concrete surfaces displayed increasingly pronounced changes in coloration as the maximum heating temperature rose. The red response became particularly evident near and above 600°C. These changes are associated with alterations in surface alkalinity and calcium-bearing hydration products, including $Ca(OH)_2$. Surface color can therefore contribute to qualitative assessment of temperature-induced damage, although it cannot determine exposure temperature or chemical composition reliably without supporting measurements.

(2) Concrete mass decreased progressively after heating, principally because moisture was released and, at elevated temperatures, additional transformations of the hydrated matrix occurred. The resulting mass-loss ratio increased with the target temperature, with a marked rise at the highest exposures. No obvious spalling was observed in the investigated specimens. This finding pertains to the particular mixture, specimen geometry, and heating procedure and does not imply that spalling will be absent under other fire conditions.

(3) The relative dynamic modulus of elasticity decreased as heating temperature increased, indicating progressive internal deterioration. Under the reported test conditions, the relative modulus after water cooling was generally higher than that following natural cooling at the higher temperatures, although both were substantially reduced. Lower ultrasonic-derived modulus values corresponded to a less continuous internal structure, making this parameter a useful supporting indicator of damage rather than a direct replacement for destructive strength testing.

(4) Thermal exposure increased cracking and altered the electrical response of concrete. Resistance increased with temperature after natural cooling, while it decreased markedly after immersion in water. This difference is consistent with the competing effects of damage to the solid skeleton and the presence or penetration of conductive pore water. The frequency of electrical measurement also influenced the reported resistance, demonstrating the need to standardize measurement conditions when comparing specimens.

(5) Residual compressive strength decreased under both cooling regimes as heating temperature increased, with the greatest deterioration occurring in the 600–800°C range. Within the measured dataset, compressive strength was related to mass loss and relative dynamic modulus of elasticity through the reported empirical linear relationships. These associations support a combined assessment using physical and mechanical indicators, while their applicability beyond the investigated concrete mixture and experimental conditions requires additional validation.

Author Contributions

Both authors contributed equally to this research and approved the final version for publication.

Conflict of Interest

The authors declare that they have no conflicts of interest.

Funding Information

This research was supported by the Youth Innovation Team of Shaanxi Universities. Additional support was acknowledged from the Support Program for Outstanding Young Talents of Shaanxi Universities (Dr. Tao Luo), the Special Fund for the Launch of Scientific Research at Xijing University (XJ18T02), and the Special Research Project of the Education Department of the Shaanxi Provincial Government (19JK0913).

Data Availability

The data are available from the corresponding author upon reasonable request.

References

[1] Xing, Z., Beaucour, A.-L., Hebert, R., Noumowe, A., & Ledesert, B. (2015). Aggregate's influence on thermophysical concrete properties at elevated temperature. *Construction and Building Materials, 95*, 18–28.

[2] Geng, J., Sun, Q., Zhang, W., & Lü, C. (2016). Effect of high temperature on mechanical and acoustic emission properties of calcareous-aggregate concrete. *Applied Thermal Engineering, 106*, 1200–1208.

[3] Ling, T.-C., Poon, C.-S., & Kou, S.-C. (2012). Influence of recycled glass content and curing conditions on the properties of self-compacting concrete after exposure to elevated temperatures. *Cement and Concrete Composites, 34*(2), 265–272.

[4] Zi, W., Yu, Z.-W., & Kuang, Y.-C. (2013). Influences of temperature and time on concrete compressive strength after water cooling. *Advanced Materials Research, 639–640*, 1021–1024.

[5] Kodur, V. K. R., & Sultan, M. A. (2003). Effect of temperature on thermal properties of high-strength concrete. *Journal of Materials in Civil Engineering, 15*(2), 101–107.

[6] Xing, Z., Beaucour, A.-L., Hebert, R., Noumowe, A., & Ledesert, B. (2011). Influence of the nature of aggregates on the behaviour of concrete subjected to elevated temperature. *Cement and Concrete Research, 41*(4), 392–402.

[7] Nazri, F. M., Shahidan, S., Baharuddin, N. K., Beddu, S., & Abu Bakar, B. H. (2017). Effects of heating durations on normal concrete residual properties: Compressive strength and mass loss. *IOP Conference Series: Materials Science and Engineering, 271*(1), Article 012013.

[8] Kizilkanat, A. B., Yüzer, N., & Kabay, N. (2013). Thermo-physical properties of concrete exposed to high temperature. *Construction and Building Materials, 45*, 157–161.

[9] European Committee for Standardization. (2004). *Eurocode 2: Design of concrete structures—Part 1-2: General rules—Structural fire design* (EN 1992-1-2:2004).

[10] Yan, J.-H., Lin, Z.-S., & Hu, Y.-C. (2002). The effects of high temperature on compressive strength of concrete [Article in Chinese]. *China Civil Engineering Journal, 35*(5), 17–19.

[11] Jia, F.-P., Lü, H.-L., Cui, Y.-L., Qu, Y.-Y., & Wang, Y.-C. (2009). Research on degradation of concrete properties after high-temperature exposure under different cooling methods [Article in Chinese]. *Journal of China University of Mining & Technology, 38*(1), 25–29.

[12] Lü, T.-Q., Zhao, G.-F., Lin, Z.-S., & Yue, Q.-R. (2003). Microscopic analysis of long-standing concrete after high temperature [Article in Chinese]. *Journal of Building Materials, 6*(2), 135–141.

[13] Bi, J., Liu, P., & Gan, F. (2020). Effects of the cooling treatment on the dynamic behavior of ordinary concrete exposed to high temperatures. *Construction and Building Materials, 248*, Article 118688.

[14] Karolina, R., & Corsika, M. S. Y. (2020). Analysis of mechanical and physical behaviour of post-burn concrete. *IOP Conference Series: Materials Science and Engineering, 725*(1), Article 012034.

[15] Cioni, P., Croce, P., & Salvatore, W. (2001). Assessing fire damage to r.c. elements. *Fire Safety Journal, 36*(2), 181–199.

[16] Du, S., Zhang, Y., Sun, Q., Gong, W., Geng, J., & Zhang, K. (2018). Experimental study on color change and compression strength of concrete tunnel lining in a fire. *Tunnelling and Underground Space Technology, 71*, 106–114.

[17] Sun, Q., Geng, J., Zhang, W., & Lü, C. (2017). Variation of wave velocity and thermal conductivity of concrete after high-temperature treatment. *Environmental Earth Sciences, 76*(2), Article 88.

[18] Hu, J., Sun, Q., Chen, S.-E., & Zhang, W. (2018). The thermodynamic properties variation of cemented clay after treatment at high temperatures. *Construction and Building Materials, 182*, 523–529.

[19] Zhang, Y., Sun, Q., & Yang, X. (2018). Changes in color and thermal properties of fly ash cement mortar after heat treatment. *Construction and Building Materials, 165*, 72–81.

[20] Chan, S. Y. N., Luo, X., & Sun, W. (2000). Effect of high temperature and cooling regimes on the compressive strength and pore properties of high performance concrete. *Construction and Building Materials, 14*(5), 261–266.

[21] Bingöl, A. F., & Gül, R. (2009). Effect of elevated temperatures and cooling regimes on normal strength concrete. *Fire and Materials, 33*(2), 79–88.

[22] Karakoç, M. B. (2013). Effect of cooling regimes on compressive strength of concrete with lightweight aggregate exposed to high temperature. *Construction and Building Materials, 41*, 21–25.

[23] Fingerloos, F., & Richter, E. (2007). Nachweis des konstruktiven Brandschutzes bei Stahlbetonstützen [Verification of structural fire protection for reinforced-concrete columns]. *Beton- und Stahlbetonbau, 102*(4), 198–206.

[24] Handoo, S. K., Agarwal, S., & Agarwal, S. K. (2002). Physicochemical, mineralogical, and morphological characteristics of concrete exposed to elevated temperatures. *Cement and Concrete Research, 32*(7), 1009–1018.

[25] He, K.-C., Guo, R.-X., Ma, Q.-M., Yan, F., Lin, Z.-W., & Sun, Y.-L. (2016). Experimental research on high temperature resistance of modified lightweight concrete after exposure to elevated temperatures. *Advances in Materials Science and Engineering, 2016*, Article 5972570.

[26] Menou, A., Mounajed, G., Boussa, H., La Borderie, C., & Lafdi, K. (2008). Thermal damage approach of concrete: Application to specimens subjected to combined compressive and high temperature loads. *High Temperature Materials and Processes, 27*(1), 23–39.

[27] Zaidi, S. K. A., Sharma, U. K., Bhargava, P., & Bhandari, N. M. (2017). An empirical model for confined concrete after exposure to high temperature. *Fire and Materials, 41*(7), 848–856.

[28] Georgali, B., & Tsakiridis, P. E. (2005). Microstructure of fire-damaged concrete: A case study. *Cement and Concrete Composites, 27*(2), 255–259.

[29] Othuman, M. A., & Wang, Y. C. (2011). Elevated-temperature thermal properties of lightweight foamed concrete. *Construction and Building Materials, 25*(2), 705–716.

[30] Luo, X., Sun, W., & Chan, S. Y. N. (2000). Effect of heating and cooling regimes on residual strength and microstructure of normal strength and high-performance concrete. *Cement and Concrete Research, 30*(3), 379–383.

[31] Wang, R., He, F., Shi, C., Zhang, D., Chen, C., & Dai, L. (2022). AC impedance spectroscopy of cement-based materials: Measurement and interpretation. *Cement and Concrete Composites, 131*, Article 104591. https://doi.org/10.1016/j.cemconcomp.2022.104591.

[32] Shen, J., Wang, S., & Xu, Q. (2024). Characterization of microstructure and moisture distribution evolution of concrete using AC impedance spectroscopy. *Journal of Building Engineering, 98*, Article 111272. https://doi.org/10.1016/j.jobe.2024.111272.